International Journal of Applied Earth Observations and Geoinformation 106 (2022) 102671

Contents lists available at ScienceDirect

International Journal of Applied Earth Observations and Geoinformation

journal homepage: www.elsevier.com/locate/jag

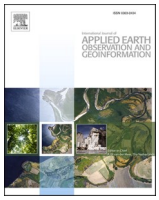

On the influence of acquisition geometry in backscatter time series over wheat

Maria Arias *, Miguel Ángel Campo-Bescós, Jesús Álvarez-Mozos

Institute for Sustainability & Food Chain Innovation (IS-FOOD), Department of Engineering, Public University of Navarre (UPNA), Arrosadía Campus, 31006 Pamplona, Spain

ARTICLE INFO

Keywords:
Azimuthal anisotropy
Incidence angle
Normalization
SAR
Sentinel-1
Wheat

ABSTRACT

Dense time series of Sentinel-1 imagery are an invaluable information source for agricultural applications. Multiple orbits can observe a specific area and their combination could improve the temporal resolution of the time series. However, the orbits have different acquisition geometries regarding incidence and azimuth angles that need to be considered. Furthermore, crops are dynamic canopies and the influence of incidence and azimuth angles might change during the agricultural season due to different phenological stages. The main objective of this letter is to evaluate the influence of different acquisition geometries in Sentinel-1 backscatter time series over wheat canopies, and to propose a strategy for their correction. A large dataset of wheat parcels (~40,000) was used and 344 Sentinel-1 images from three relative orbits were processed during two agricultural seasons. The first analysis was a monthly evaluation of the influence of incidence angle on backscatter (σ^0) and terrain flattened backscatter (γ^0). It showed that terrain flattening significantly reduced the backscatter dependence on incidence angle, being negligible in VH polarization but not completely in VV polarization. Incidence angle influence in VV backscatter changed in time due to wheat growth dynamics. To further reduce it, an incidence angle normalization technique followed by an azimuthal anisotropy correction were applied. In conclusion, γ^0 enabled a reasonable combination of different relative orbits, that may be sufficient for many applications. However, for detailed analyses, the correction techniques might be implemented to further reduce orbit differences, especially in bare soil periods or winter months.

1. Introduction

Synthetic aperture radar (SAR) imagery has proven to be useful for agricultural applications (Liu et al., 2019), such as crop classification, yield forecasting or soil moisture estimation (Steele-Dunne et al., 2017). The launch of the Sentinel-1 mission in 2014 made freely available an unprecedented collection of worldwide systematically collected C-band observations (Berger et al., 2012). Currently, the mission consists of two twin satellites that allow a nominal temporal resolution of 6 days. Yet, there can be multiple orbits with different acquisition geometries (incidence and azimuth angles) observing a specific area, whose combination can reduce the revisit time to less than two days in many parts of Europe (Weiß et al., 2021). These denser time series could be interesting for several different applications. However, the combination of time series acquired with different orbits might not be so straightforward, due to the sensitivity of backscatter to image geometry, mainly incidence and azimuth angle variations (Bartalis et al., 2006; Gauthier et al., 1998; Rizzoli and Bräutigam, 2014; Ulaby et al., 1982).

In effect, observed backscatter values vary depending on the incidence angle (Ulaby et al., 1982). However, the magnitude of these variations depend on target characteristics and scattering mechanisms (Ardila et al., 2010). Smooth targets dominated by the specular component of surface scattering were found to be particularly sensitive to incidence angle variations (Skriver et al., 1999). Conversely, very rough soils or vegetation covers, where volume scattering predominates, have a lower incidence angle dependence. Similarly, azimuthal effects are more prominent in surface scattering situations with predefined directional structures. Certainly, both incidence and azimuth angle effects increase in areas with moderate to strong topography.

Different methods exist to normalize the incidence angle influence on backscatter. One of the most common techniques is the cosine correction (Ulaby et al., 1982), based on Lambert's law for optics, that was also modified to account for the dynamics of maize (Feng et al., 2021). Other methods are based on regression analysis (Phung et al.,

* Corresponding author.
E-mail address: maria.arias@unavarra.es (M. Arias).

https://doi.org/10.1016/j.jag.2021.102671
Received 12 November 2021; Received in revised form 22 December 2021; Accepted 28 December 2021
Available online 5 January 2022

2020; Wagner et al., 1999), statistical techniques (Mladenova et al., 2013; Ye et al., 2015), on the backscatter and incidence angle product (Kaplan et al., 2021), on radiative-transfer models (Ardila et al., 2010) or on empirical relationships with NDVI (Fieuzal et al., 2013). Regarding the correction of azimuthal effects, Schaufer et al. (2018) found that azimuthal anisotropy was mainly caused by the orientation of topographic slopes and proposed a matching method for its correction. However, some studies identified a different azimuthal behavior for different land covers (Bartalis et al. 2006), and eventually a reduced influence of azimuthal angles for wheat when compared to incidence angle variations (Weiß et al., 2021). On the other hand, Small (2011) proposed a radiometric terrain correction method that 'flattens' backscatter values and potentially enables the combined use of multi-track and multi-sensor backscatter time series.

The case of agricultural land-covers is peculiar, since most crops are dynamic targets, and thus scattering mechanisms change during the agricultural season. This might change the influence of incidence and azimuth angle in backscatter. Wheat is one of the main crops cultivated worldwide, with more than 200 million ha cultivated per year (FAOSTAT, 2021), and it has been extensively investigated using remote sensing data, in particular SAR data (Liu et al., 2019). Despite its global importance, the effect of incidence and azimuth angle variations in backscatter time series, and the dynamics of these effects during the growing season of wheat have not been sufficiently studied. Therefore, the objective of this letter is to evaluate the influence of incidence and azimuth angles on Sentinel-1 backscatter time series acquired over wheat fields with different orbits, and to propose a strategy for their correction.

2. Study area and data

2.1. Study area

The study area corresponds to the agricultural areas of the province of Navarre (Northern Spain) (N42°40′4.8″ and W1°38′52.8″). This province is relatively small (10,391 km^2), but the diversity of landscape and climate conditions creates regions with marked differences in terms of cropping patterns and agricultural management strategies, and as a result the province can be divided into seven agricultural regions (Arias et al., 2020).

2.2. Sentinel-1 images

All available Sentinel-1A and B ground range detected (GRD) images covering Navarre from 1 September 2016 to 31 August 2018 were used for the analysis. These corresponded to one ascending node (103ASC) and two descending nodes (8DESC and 81DESC). In total, 344 images were used. The median incidence angle for 103ASC was 41°, for 8DESC was 43° and for 81DESC was 34°.

Scenes were processed using an automated pipeline in SNAP Graph Processing Toolbox that followed this process: 1) thermal noise removal; 2) slice assembly; 3) apply orbit file; 4) calibration; 5) speckle filtering (3x3 Gamma-MAP); 6) range-doppler terrain correction and 7) subset to the extent of Navarre. This process produced σ^0 backscatter values in dB units. A second processing chain was implemented including the terrain flattening algorithm (Small, 2011) and resulting in γ^0 backscatter coefficients (in dB units too). For the terrain flattening and terrain correction steps the SRTM 1sec HGT DEM was used. The resulting images had an output pixel size of 20 m. As an additional output, the local incidence angle map was generated for each scene, and used for subsequent analyses. For conciseness, the local incidence angle will be referred to as incidence angle in the article.

2.3. Wheat parcels dataset

Wheat is cultivated as a winter crop in Navarre. It is typically sown in the months of October or November and harvested at the end of June or in the first week of July. All wheat parcels for agricultural years 2017 and 2018 were extracted from the EU Common Agricultural Policy (CAP) declarations database provided, as an anonymized version, by the Agricultural Department of the Government of Navarre. A 5 m inner buffer was applied to the vector file and parcels smaller than 0.5 ha were discarded. The median backscatter time series per parcel were calculated for each orbit. With the aim to exclude parcels that might be wrongly declared as wheat, 10% of parcels most dissimilar to the typical (median) wheat time series were masked out (Arias et al., 2020). The final number of wheat parcels used was 18,750 for 2017 and 20,374 for 2018.

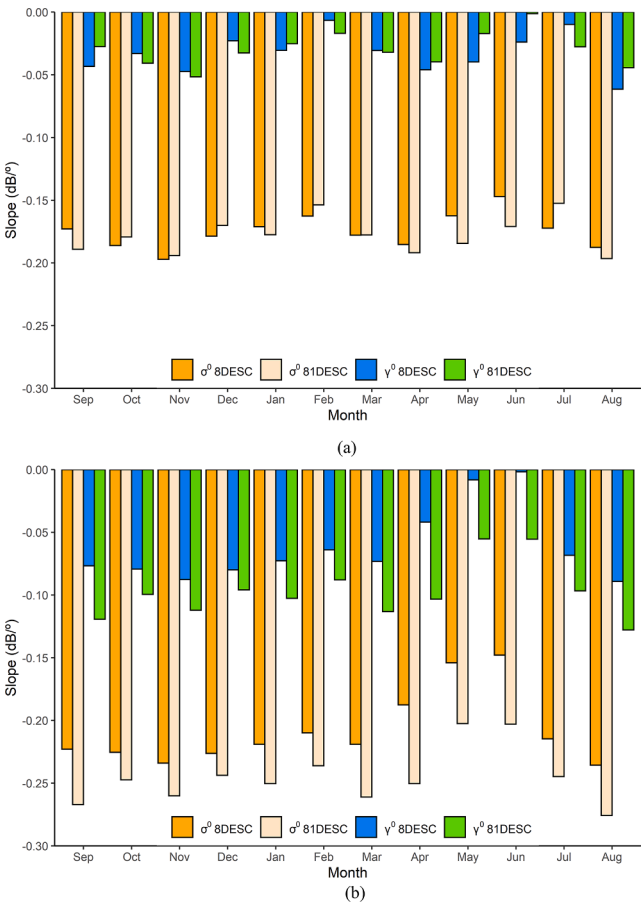

Fig. 1. Monthly slope for wheat parcels. The slope accounts for the linear relationship between backscatter and incidence angle. (a) Slope for VH polarization. (b) Slope for VV polarization.

2.4. Incidence angle influence on backscatter

As a preliminary analysis, the dependency of σ^0 and γ^0 on the incidence angle (θ_{loc}) was evaluated by means of the slope of the linear regressions $\sigma^0 = f(\theta_{loc})$ and $\gamma^0 = f(\theta_{loc})$ fitted for each month. For this, the two descending orbits (8DESC and 81DESC) were taken into account, covering the complete growth cycle of wheat in Navarre. There, the season starts in September and ends in August the year after. Therefore, this monthly evaluation comprised both periods of bare and vegetated soils.

Results (Fig. 1) showed clear differences between the slope values obtained for σ^0 and γ^0 backscatter, with typical slope values in VV polarization of − 0.25 dB/° for σ^0 that decreased to − 0.10 dB/° for γ^0. For VH polarization slope values (in absolute terms) were smaller but differences between σ^0 and γ^0 backscatter were similar, with slope values of −0.18 dB/° for σ^0 and −0.03 dB/° for γ^0. Therefore, the influence of the

incidence angle in backscatter significantly decreased when the terrain flattening process was applied. Yet, some residual influence seemed to be present.

There were clear differences between VH and VV polarizations (Fig. 1). The slope values were much smaller for VH. The mean slope value of −0.03 dB/° for γ^0, indicated an almost negligible influence of the incidence angle in γ^0 for this polarization. In VV, the obtained slope values were larger, illustrating that the influence of the incidence angle on backscatter remained after terrain flattening. Slope values were slightly larger for the 81DESC orbit that had lower incidence angles. For VV polarization, slope values varied during the year. The largest values were achieved in periods of smooth bare soils (e.g., November after sowing or August after harvest) (∼-0.23 dB/° for σ^0 and ∼ -0.10 dB/° for γ^0) that decreased steadily with wheat growth reaching a minimum in May and June (∼-0.16 dB/° for σ^0 and ∼ -0.04 dB/° for γ^0). In these months, wheat canopy was at its maximum (BBCH growth stages 5–8) and the incidence angle influence was negligible.

This preliminary analysis recommends applying the terrain flattening algorithm whenever incidence angle variations are significant. Yet, some influence remains, so, for detailed analyses an incidence angle normalization might be applied to remove eventual biases in VV backscatter. Furthermore, this normalization should take into account the dynamic nature of crops and the variations in $\gamma^0 = f(\theta_{loc})$ relationship during the year.

3. Methodology

3.1. Backscatter sample selection

The objective of this analysis is to normalize γ^0 VV backscatter time series obtained in different orbits, so that they can be used in further analyses as a single time series. To evaluate the success of the normalization, a backscatter sample selection is done, selecting for each parcel acquisitions of different orbits obtained in a small time-frame. Ideally, in case simultaneous acquisitions were available, eventual biases between acquisitions would fade after a successful normalization. Longer time-frames enhance the probability of backscatter variations between orbits due to other 'disturbing' factors (e.g., precipitation). Orbits 8DESC and 103ASC overpassed the study area the same days at 6:00 and 18:00, respectively; and orbit 81DESC 24 h before 8DESC, and thus 36 h before 103ASC. Since significant changes in wheat conditions are not expected in 36 h, backscatter values in this time-frame are considered comparable unless a strong weather event or agricultural practice (e.g., tillage or harvest) occurred in between. Thus, to mask out these eventual disturbing factors, for each parcel, dates with a γ^0 backscatter difference between orbit pairs larger than 3 dB were excluded from the analysis. This excluded only ∼ 15% of the data. To summarize, for each wheat parcel a sample of backscatter triplets (in orbits 8DESC, 81DESC and 103ASC) acquired during the two agricultural seasons was extracted and this formed the basis for all subsequent analyses.

3.2. Incidence angle normalization

The goal of normalization techniques is to remove the contribution of the incidence angle to the total backscatter. Mladenova et al. (2013) proposed a technique based on a histogram matching procedure that can account for the nonlinear nature of backscatter – incidence angle relationship. In this study, this technique was applied individually for the different periods explained below. The large dataset used in this study allowed calculating the statistics needed for the histogram normalization at the agricultural region scale, as follows:

$$\gamma^0(ref) = \overline{\gamma}^0_{ref} + \widehat{\gamma}^0_{ref}\frac{(\gamma^0 - \overline{\gamma}^0)}{\widehat{\gamma}^0} \quad (1)$$

where γ^0 is radar backscatter in [dB]; '–' and '^' indicate mean and standard deviation for each 1° incidence angle bin; and *ref* refers to reference angle. The reference angle was selected as the median incidence angle of the three orbits. As a result, the 40° reference angle was chosen.

Considering the different backscatter dependence on incidence angle (Fig. 1), two periods were considered: May-June and the rest of the year.

3.3. Azimuthal anisotropy correction

After incidence angle normalization, backscatter time series acquired in ASC and DESC orbits were subsequently processed to correct their eventual differences due to their different observation directions (azimuthal anisotropy) following Schaufler et al. (2018) . If no azimuthal anisotropy existed, the orbits' means should be the same:

$$\overline{\gamma}^0(40^o)_{103ASC} = \overline{\gamma}^0(40^o)_{8DESC} = \overline{\gamma}^0(40^o)_{81DESC} \quad (2)$$

To achieve this, the azimuthal correction method (Schaufler et al., 2018) computes first a reference backscatter value as the mean of all backscatter data from the three orbits:

$$\gamma^0_{ref} = \overline{\gamma}^0(40^o) \quad (3)$$

Then, the difference between this reference value and the mean of each orbit is the correction factor d_{orbit} necessary to compensate azimuthal effects:

$$d_{orbit} = \gamma^0_{ref} - \overline{\gamma}^0(40^o)_{orbit} \quad (4)$$

The azimuthal anisotropy is finally corrected by adding d_{orbit} to each normalized backscatter value:

$$\gamma^0(40^o)_{az\_corr} = \gamma^0(40^o)_{orbit} + d_{orbit} \quad (5)$$

All the normalized backscatter data from section 3.2. were processed with this algorithm. The two periods were also separated for the anisotropy correction.

3.4. Evaluation of results

A successful correction of incidence angle and azimuthal anisotropy contributions would produce the same parcel scale backscatter values acquired in different orbits within the established 36 h time-frames. Therefore, the absolute backscatter difference ($|\Delta|$) from the three orbits was used as an evaluation criteria. The $|\Delta|$ between orbits were computed pairwise (8DESC-103ASC, 8DESC-81DESC and 81DESC-103ASC) for each parcel. These $|\Delta|$ values were grouped per month to illustrate the performance of the correction methods throughout the year.

Additionally, the performance of the corrections was evaluated using the correlation between backscatter and Red-edge NDVI (reNDVI) (Gitelson and Merzlyak, 1994). The rationale of this comparison is that if the applied corrections successfully reduced angular effects, then the correlation with reNDVI should improve. For this, a ∼ 270 km^2 pilot zone was selected (N42°42′53.6′′ and W1°16′12.7′′), containing 855 wheat parcels with different topographic orientations and slopes. Sentinel-2 scenes were searched, but cloud affection is typically persistent during wheat growing cycle in Navarre. Therefore, the correlation was assessed for a complete agricultural campaign (2018), but also focusing only on its final part, i.e. April-July, where the availability of cloud-free scenes improves. This period includes crop maturity, senescence and harvest. In total, 14 cloud-free Sentinel-2 Level-2A scenes were obtained. The median reNDVI time series for each parcel were obtained and interpolated for Sentinel-1 acquisition dates. The Pearson correlation coefficient R was computed between the interpolated reNDVI time series and all the backscatter time series (σ^0, γ^0, $\gamma^0(40°)$ and $\gamma^0(40°)_{az\_corr}$).

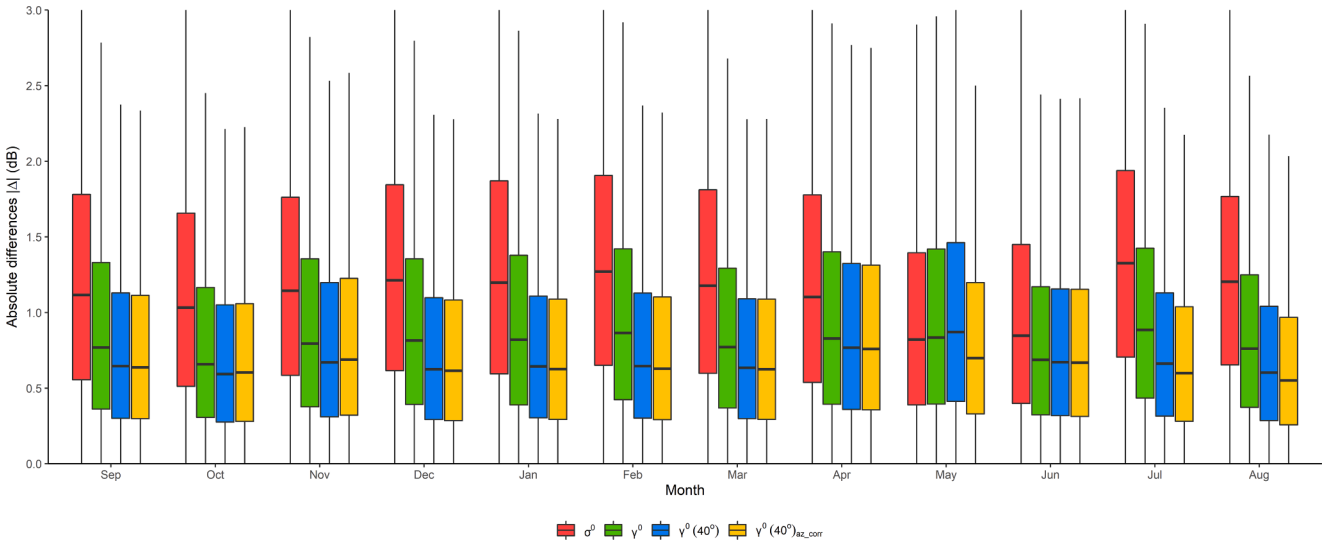

Fig. 2. Boxplots of absolute backscatter differences for the three orbits during the year and considering different processing alternatives.

4. Results and discussion

Fig. 2 represents the |Δ| values for all wheat fields during the season and for the four different processing alternatives considered: σ^0, γ^0, $\gamma^0(40°)$ and $\gamma^0(40°)_{az\_corr}$. σ^0 backscatter had the highest |Δ| values, with a median of 1.25 dB that represented the significant influence of incidence angle variations in backscatter. γ^0 presented a median |Δ| of 0.80 dB, with October and June being the months with the lowest values (~0.67 dB). The significant reduction of |Δ| (~0.45 dB) for γ^0 (Fig. 2), illustrated the effectiveness of terrain flattening for compensating incidence angle variations in backscatter data, in accordance with Fig. 1.

|Δ| decreased slightly further after incidence angle normalization ($\gamma^0(40°)$), with a reduction of 0.15 dB compared to γ^0, and also after azimuthal anisotropy correction ($\gamma^0(40°)_{az\_corr}$), where |Δ| achieved an additional reduction of 0.02 dB. Both corrections were effective but the reduction was much lower than the initial reduction achieved after terrain flattening. The intensity of the incidence angle normalization differed between months, and was highest for months with no vegetation, i.e., July, August; and winter months (BBCH growth stages 1–2), where the reductions of |Δ| were greater than 0.16 dB. For May and June $\gamma^0(40°)$ had almost no effect in |Δ|, due to the reduced effect of the incidence angle in backscatter during these months (Fig. 1). Conversely, $\gamma^0(40°)_{az\_corr}$ was most effective in May, compensating the under-correction of γ^0 and $\gamma^0(40°)$. In summary, the median |Δ| for all the months was 0.65 dB for $\gamma^0(40°)$, and 0.63 dB for $\gamma^0(40°)_{az\_corr}$.

When evaluating |Δ| values per month, it was possible to observe that the period after harvest (July and August) achieved the highest |Δ| reductions after both corrections (greater than0.21 dB). In September, October and November, corrections had a smaller effect (~0.10 dB). During these months sowing occurs, leading to a higher soil roughness variability between different parcels that might mask potential improvements for individual parcels. Tilled or newly sown soils have a more Lambertian behavior, leading to a lower influence of incidence angle (Ulaby et al., 1982). December, January and February were the months that presented the highest |Δ| in the original data and achieved a good reduction of differences after incidence angle normalization (~0.20 dB). In March and April no significant improvements were detected (<0.14 dB). This could be explained by the dynamics of VV backscatter during wheat growth cycle. Once wheat initiates the stem elongation stage, an attenuation of VV backscatter occurs (Mattia et al., 2003), leading to lower differences between subsequent acquisitions. May and June were the months with the lowest influence of incidence

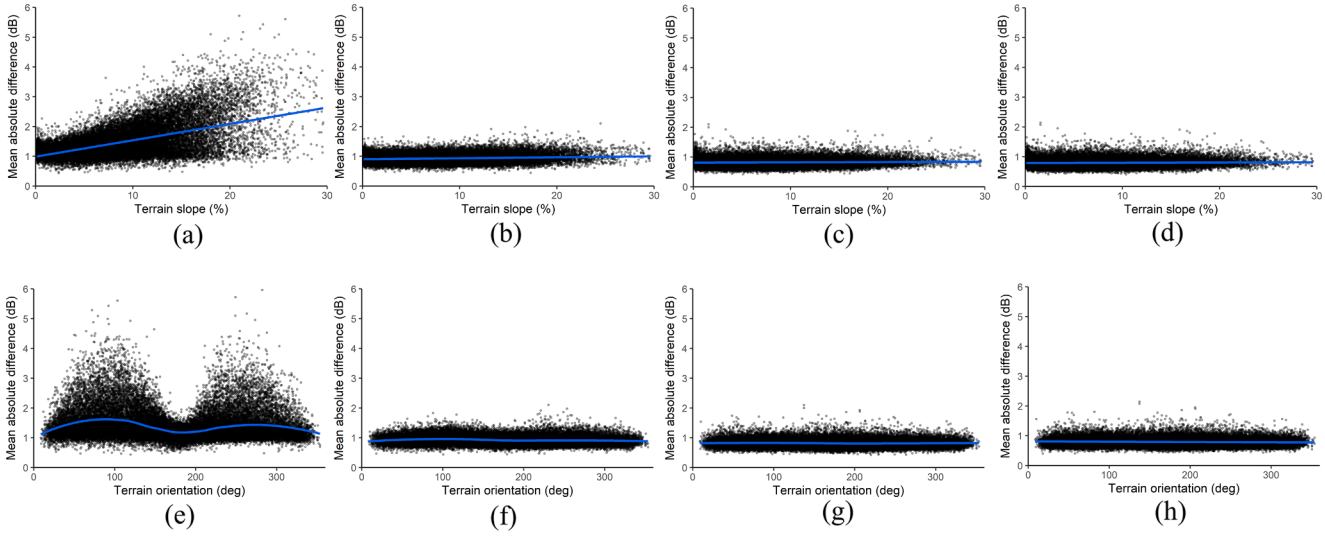

Fig. 3. Dependence of mean absolute backscatter difference of wheat parcels on terrain slope (upper row) and orientation (lower row); for the different backscatter outputs investigated: (a, e) σ^0, (b, f) γ^0, (c, g) $\gamma^0(40°)$, (d, h) $\gamma^0(40°)_{az\_corr}$.

Table 1
Pearson correlation coefficient of reNDVI and backscatter time series for the pilot zone.

Backscatter correction	Full campaign	Maturity to harvest
σ^0	−0.396	−0.587
γ^0	−0.417	−0.662
$\gamma^0(40°)$	−0.419	−0.686
$\gamma^0(40°)_{az\_corr}$	−0.419	−0.686

angle. While the anisotropy corrections achieved a certain decrease of $|\Delta|$ in May (0.13 dB), there was little improvement in June (0.02 dB).

Exploring the influence of terrain slope and orientation on the mean $|\Delta|$ of each wheat parcel (Fig. 3) it can be observed that terrain flattening successfully reduced the majority of the radiometric effect of topography. Yet a residual dependence remained, which could be further reduced with the incidence angle and azimuth anisotropy corrections.

The correlation results for reNDVI and backscatter (Table 1) showed a negative correlation that responded to the typical backscatter pattern of wheat at VV polarization (Mattia et al., 2003). Correlation values for the full campaign were rather low, but when focusing on the period between maturity and harvest it improved as a consequence of the rising backscatter values at this period (Brown et al., 2003; Veloso et al., 2017) and the rapid decrease of reNDVI at crop ripening and senescence (Fig. 4). The improvements in correlation were minor for the full campaign (from 0.40 to 0.42), but more significant from maturity to harvest (from 0.59 to 0.69). These results demonstrate that the corrections applied (in particular γ^0 and $\gamma^0(40°)$) enhance the correlation with optical vegetation indices, and hence provide a better description of wheat growth. Yet, further studies in areas with a higher availability of optical data should be performed to confirm these results.

The backscatter time series (Fig. 4) showed that the corrections were successful as they not only improved the matching of the three orbits but also reduced backscatter variability (error bars), since their eventual differences due to angular effects also decreased.

Taking into account that Sentinel-1 radiometric accuracy is 1 dB (Berger et al., 2012), for some applications terrain flattened backscatter (γ^0) computed for different orbits might be comparable without further processing given the relatively low influence of acquisition geometry in the values observed here. However, for quantitative analyses requiring more detail (e.g. soil moisture retrieval) or when different orbits need to be combined to enhance the temporal resolution, a closer match between these orbits might be achieved by implementing incidence angle normalization and azimuthal anisotropy correction techniques (Bauer-Marschallinger et al., 2021). Our results, validate the correction methods applied (Mladenova et al., 2013; Schaufler et al., 2018; Small, 2011) and recommend their implementation in image processing pipelines and software. Coinciding with our results, recently (d'Andrimont et al., 2021), the importance of terrain flattening and incidence and azimuth angle corrections for operational applications of Sentinel-1 data was stressed out, in particular for crops with prolonged bare soil phases.

Although a general idea is that agricultural lands occupy flat terrains, in many parts of the world, farmers cultivate areas that have significant slopes, making these corrections necessary even when working with a single orbit, as our results confirm. In particular, it is shown that for wheat the incidence angle influence on backscatter changes during the season due to its phenological development. Similar studies in other crops are recommended to confirm this finding.

5. Conclusion

In this study, the influence of acquisition geometry (incidence and azimuth angles) on backscatter (σ^0) and terrain flattened backscatter (γ^0) was evaluated for wheat parcels. The analysis revealed that terrain flattening markedly reduced the influence of incidence angle in VH and

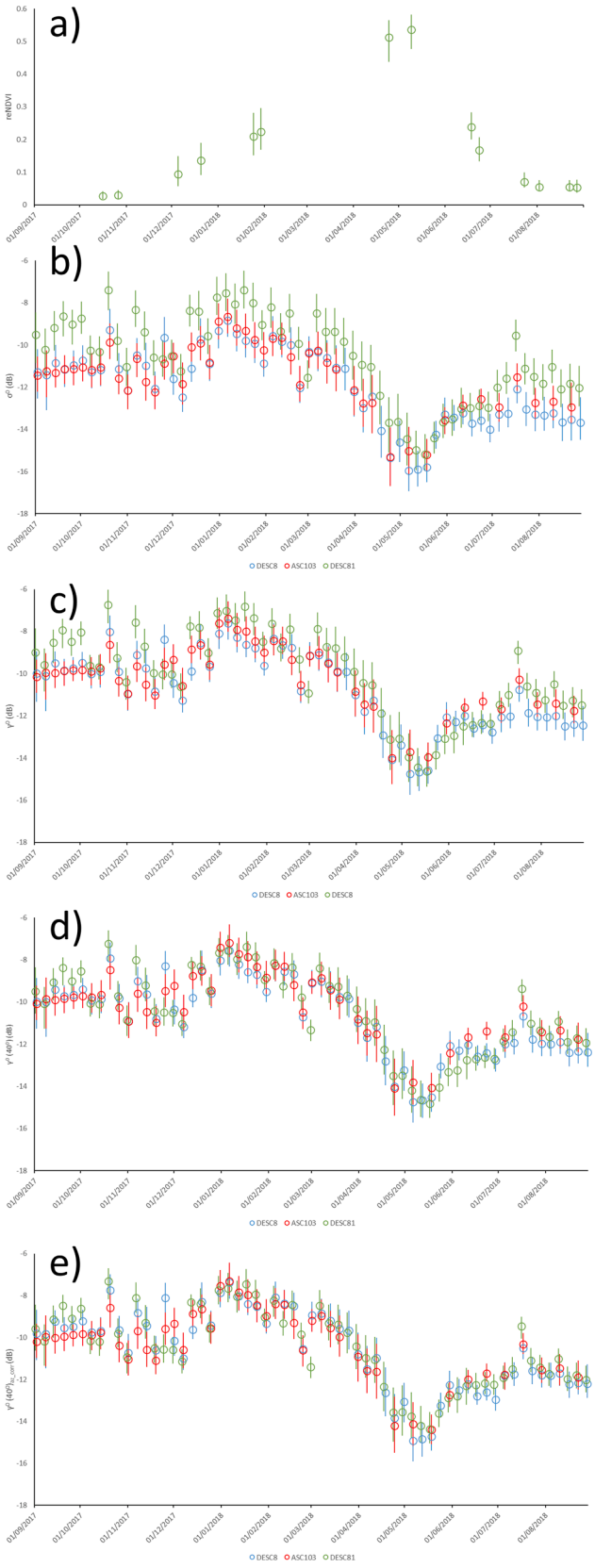

Fig. 4. Median time series of reNDVI and backscatter for wheat parcels in the pilot zone. The error bars represent the interquartile range (IQR): (a) reNDVI (b) σ^0, (c) γ^0, (d) $\gamma^0(40°)$, (e) $\gamma^0(40°)_{az\_corr}$. Colors in b, c, d and e represent the different orbits.

VV polarizations, being almost negligible for VH polarization. In VV polarization, the influence of the incidence angle slightly remained, although it varied along the growing season, being the least when the crop canopy was fully grown. It was thus demonstrated that the incidence angle influence on backscatter varied due to the phenological development of the crop.

The analysis of backscatter differences between the three relative orbits studied, showed that terrain flattening could achieve a significant reduction of angle variations in backscatter data. Yet, incidence angle normalization could further reduce backscatter differences, particularly in winter months and bare soil periods. The correlation with reNDVI also improved after terrain flattening and normalization, revealing a better description of wheat growth. The azimuth anisotropy correction had a lower effect that was mainly relevant in May. The differences between ascending and descending passes might be partly due to the acquisition geometry (incidence and azimuth angles) and partly due to the time of the day (eventually dew, frost, soil moisture, etc.), but this has not been sufficiently studied yet.

For applications where different orbits have to be combined, the need to further correct terrain-flattened backscatter values will depend on the level of precision required. Furthermore, for quantitative studies aiming at retrieving a bio-geophysical variable of interest (e.g., soil moisture), adding these corrections might provide enhanced results.

CRediT authorship contribution statement

Maria Arias: Data curation, Formal analysis, Investigation, Methodology, Software, Visualization, Writing – original draft. **Miguel Ángel Campo-Bescós:** Supervision, Writing – review & editing. **Jesús Álvarez-Mozos:** Conceptualization, Funding acquisition, Investigation, Methodology, Project administration, Resources, Supervision, Writing – review & editing.

Declaration of Competing Interest

The authors declare that they have no known competing financial interests or personal relationships that could have appeared to influence the work reported in this paper.

Acknowledgements

The authors would like to acknowledge the Government of Navarre for providing the (CAP) declarations database used in this research.

Funding: This work was supported by the Spanish Ministry of Economy and Competitiveness and the European Regional Development Fund (MINECO/FEDER-UE) through projects [CGL2016-75217-R and PID2019-107386RB-I00 / AEI / 10.13039/501100011033] and doctoral grant [BES-2017-080560].

References

Ardila, J.P., Tolpekin, V., Bijker, W., 2010. Angular backscatter variation in L-band ALOS ScanSAR images of tropical forest areas. IEEE Geosci. Remote Sens. Lett. 7 (4), 821–825. https://doi.org/10.1109/LGRS.2010.2048411.

Arias, M., Campo-Bescós, M.Á., Álvarez-Mozos, J., 2020. Crop Classification Based on Temporal Signatures of Sentinel-1 Observations over Navarre Province. Spain. Remote Sens. 12 (2), 278. https://doi.org/10.3390/rs12020278.

Bartalis, Z., Scipal, K., Wagner, W., 2006. Azimuthal anisotropy of scatterometer measurements over land. IEEE Trans. Geosci. Remote Sens. 44 (8), 2083–2092. https://doi.org/10.1109/TGRS.2006.872084.

Bauer-Marschallinger, B., Cao, S., Navacchi, C., Freeman, V., Reuß, F., Geudtner, D., Rommen, B., Vega, F.C., Snoeij, P., Attema, E., Reimer, C., Wagner, W., 2021. The normalised Sentinel-1 Global Backscatter Model, mapping Earth's land surface with C-band microwaves. Sci. Data 8, 1–18. https://doi.org/10.1038/s41597-021-01059-7.

Berger, M., Moreno, J., Johannessen, J.A., Levelt, P.F., Hanssen, R.F., 2012. ESA's sentinel missions in support of Earth system science. Remote Sens. Environ. 120, 84–90. https://doi.org/10.1016/j.rse.2011.07.023.

Brown, S.C.M., Quegan, S., Morrison, K., Bennett, J.C., Cookmartin, G., 2003. High-resolution measurements of scattering in wheat canopies - Implications for crop parameter retrieval. IEEE Trans. Geosci. Remote Sens. 41 (7), 1602–1610. https://doi.org/10.1109/TGRS.2003.814132.

d'Andrimont, R., Verhegghen, A., Lemoine, G., Kempeneers, P., Meroni, M., van der Velde, M., 2021. From parcel to continental scale – A first European crop type map based on Sentinel-1 and LUCAS Copernicus in-situ observations. Remote Sens. Environ. 266, 112708. https://doi.org/10.1016/j.rse.2021.112708.

Feng, Z., Zheng, X., Li, L., Li, B., Chen, S.i., Guo, T., Wang, X., Jiang, T., Li, X., Li, X., 2021. Dynamic cosine method for normalizing incidence angle effect on C-band radar backscattering coefficient for maize canopies based on NDVI. Remote Sens. 13 (15), 2856. https://doi.org/10.3390/rs13152856.

Fieuzal, R., Baup, F., Marais-Sicre, C., 2013. Monitoring wheat and rapeseed by using synchronous optical and radar satellite data—From temporal signatures to crop parameters estimation. Adv. Remote Sens. 02 (02), 162–180. https://doi.org/10.4236/ars.2013.22020.

Food and Agriculture Organization of the United Nations, 2021. FAOSTAT [WWW Document]. https://www.fao.org/faostat/en/#data/QCL.

Gauthier, Y., Bernier, M., Fortin, J.-P., 1998. Aspect and incidence angle sensitivity in ers-1 sar data. Int. J. Remote Sens. 19 (10), 2001–2006. https://doi.org/10.1080/014311698215117.

Gitelson, A., Merzlyak, M.N., 1994. Spectral Reflectance Changes Associated with Autumn Senescence of Aesculus hippocastanum L. and Acer platanoides L. Leaves. Spectral Features and Relation to Chlorophyll Estimation. J. Plant Physiol. 143 (3), 286–292. https://doi.org/10.1016/S0176-1617(11)81633-0.

Kaplan, G., Fine, L., Lukyanov, V., Manivasagam, V.S., Tanny, J., Rozenstein, O., 2021. Normalizing the local incidence angle in sentinel-1 imagery to improve leaf area index, vegetation height, and crop coefficient estimations. Land 10 (7), 680. https://doi.org/10.3390/land10070680.

Liu, C.-a., Chen, Z.-X., Shao, Y., Chen, J.-S., Hasi, T., Pan, H.-Z., 2019. Research advances of SAR remote sensing for agriculture applications: A review. J. Integr. Agric. 18 (3), 506–525. https://doi.org/10.1016/S2095-3119(18)62016-7.

Mattia, F., Le Toan, T., Picard, G., Posa, F.I., D'Alessio, A., Notarnicola, C., Gatti, A.M., Rinaldi, M., Satalino, G., Pasquariello, G., 2003. Multitemporal C-band radar measurements on wheat fields. IEEE Trans. Geosci. Remote Sens. 41, 1551–1560. https://doi.org/10.1109/TGRS.2003.813531.

Mladenova, I.E., Jackson, T.J., Bindlish, R., Hensley, S., 2013. Incidence angle normalization of radar backscatter data. IEEE Trans. Geosci. Remote Sens. 51 (3), 1791–1804. https://doi.org/10.1109/TGRS.2012.2205264.

Phung, H.-P., Nguyen, L.-D., Thong, N.-H., Thuy, L.-T., Apan, A.A., 2020. Monitoring rice growth status in the Mekong Delta, Vietnam using multitemporal Sentinel-1 data. J. Appl. Remote Sens. 14, 1. https://doi.org/10.1117/1.jrs.14.014518.

Rizzoli, P., Bräutigam, B., 2014. Radar backscatter modeling based on global TanDEM-X mission data. IEEE Trans. Geosci. Remote Sens. 52 (9), 5974–5988. https://doi.org/10.1109/TGRS.2013.2294352.

Schaufler, S., Bauer-Marschallinger, B., Hochstöger, S., Wagner, W., 2018. Modelling and correcting azimuthal anisotropy in sentinel-1 backscatter data. Remote Sens. Lett. 9 (8), 799–808. https://doi.org/10.1080/2150704X.2018.1480071.

Skriver, H., Thoug, M., G, a.,, 1999. Multitemporal C- and L-Band Polarimetric Signatures of Crops. IEEE Trans. Geosci. Remote Sens. 37, 2413–2429.

Small, D., 2011. Flattening gamma: Radiometric terrain correction for SAR imagery. IEEE Trans. Geosci. Remote Sens. 49 (8), 3081–3093. https://doi.org/10.1109/TGRS.2011.2120616.

Steele-Dunne, S.C., McNairn, H., Monsivais-Huertero, A., Judge, J., Liu, P.W., Papathanassiou, K., 2017. Radar remote rensing of agricultural canopies: A review. IEEE J. Sel. Top. Appl. Earth Obs. Remote Sens. 10, 2249–2273. https://doi.org/10.1109/JSTARS.2016.2639043.

Ulaby, F.T., Moore, R.K., Fung, A.K., 1982. Microwave Remote Sensing: Active and Passive, Vol, II. ed. Addison-Wesley, Boston, MA, Reading, MA.

Veloso, A., Mermoz, S., Bouvet, A., Le Toan, T., Planells, M., Dejoux, J.F., Ceschia, E., 2017. Understanding the temporal behavior of crops using Sentinel-1 and Sentinel-2-like data for agricultural applications. Remote Sens. Environ. 199, 415–426. https://doi.org/10.1016/j.rse.2017.07.015.

Wagner, W., Lemoine, G., Rott, H., 1999. A method for estimating soil moisture from ERS Scatterometer and soil data. Remote Sens. Environ. 70 (2), 191–207. https://doi.org/10.1016/S0034-4257(99)00036-X.

Weiß, T., Ramsauer, T., Jagdhuber, T., Löw, A., Marzahn, P., 2021. Sentinel-1 backscatter analysis and radiative transfer modeling of dense winter wheat time series. Remote Sens. 13, 1–25. https://doi.org/10.3390/rs13122320.

Ye, N., Walker, J.P., Rudiger, C., 2015. A Cumulative Distribution Function Method for Normalizing Variable-Angle Microwave Observations. IEEE Trans. Geosci. Remote Sens. 53 (7), 3906–3916.